Vol. 44, No. 3 (2022) 434-448, DOI: 10.24874/ti.1177.08.21.04

Tribology in Industry

www.tribology.rs

RESEARCH

TIG Welding Methods of Repairing Steel Components with Stainless Steel Coatings

Magdaline N. Muigai[a], Fredrick M. Mwema[a,b,*], Esther T. Akinlabi[c], Tien-Chien Jen[b], Olawale S. Fatoba[b], Tshenolo P. Leso[d], Japheth O. Obiko[e], Percy Mphasha[f]

[a]*Department of Mechanical Engineering, Dedan Kimathi University of Technology, Nyeri, Kenya,*
[b]*Department of Mechanical Engineering Science, University of Johannesburg, Auckland Park Kingsway, South Africa,*
[c]*Pan African University for Life and Earth Sciences Institute (PAULESI), Ibadan, Nigeria,*
[d]*Chemical, Materials & Metallurgical Engineering, Botswana International University of Science & Technology, Palapye, Botswana,*
[e]*Department of Mining, Materials and Petroleum Engineering, Jomo Kenyatta University of Agriculture and Technology, Nairobi, Kenya,*
[f]*School of Chemical and Metallurgical Engineering, University of the Witwatersrand, Johannesburg, South Africa.*

Keywords:

TIG welding
Wear
Corrosion
Repair welding
Surface engineering

* Corresponding author:

Fredrick M. Mwema
E-mail: fredrick.mwema@dkut.ac.ke

Received: 29 August 2021
Revised: 12 November 2021
Accepted: 16 April 2022

A B S T R A C T

Structural steel components tend to wear when exposed to corrosive and cyclic loading environments. These components can be repaired by welding on failure. This study studied the weld parameters and weld quality (porosity, depth of penetration, and coating thickness), hardness, corrosion, and wear resistance during repair welding. Mild steel samples were weld coated by varying alternating (AC) and direct (DC) currents: 40 A, 50 A, 55 A, 60 A, 65 A, and 70 A. The base material used was AISI 1045 steel, and Castolin 6825 was used as the welding electrode. The results showed that three wear mechanisms were dominant: abrasion, adhesion, and delamination. The porosity in the coated samples increased with increasing currents for both AC and DC. The welding current and current type influenced the coating thickness and penetration depth. When dipped in warm NaCl solution, the corrosion mechanism experienced by both sets of coated samples was pitting corrosion. In both cases (alternating and direct currents), the hardness values increased towards the coating surface from the substrate.

1. INTRODUCTION

Welding technology is mainly used in the joining of metallic parts [1], and some of the welding techniques used include; oxyacetylene welding, arc welding, laser-based welding, resistance welding, solid-state welding, etc. [2,3]. Metal arc welding is one of the most common welding techniques, and there are three methods of arc welding, which include Tungsten Inert Gas (TIG) welding, Metal Inert Gas (MIG) welding, and Plasma Arc (PAW) welding [4]. TIG welding has superior advantages over the other arc welding techniques [5,6], and these advantages include the ability to weld within

a controlled atmosphere and the ease of controlling various welding parameters such as current and voltage [7]. Researchers have investigated how welding parameters affecting TIG welding can be optimised [8].

Apart from joining metals, welding is used to repair worn-out steel components such as excavation buckets, shafts, pipes, and gear teeth [9-11]. These components work under extreme conditions and usually fail due to corrosion, fatigue, and wear [1]. For instance, gear teeth in an automotive gearbox experience wear, and after some time in service, the gear teeth wear out, affecting the power transmission system efficiency [12,13]. When that happens, especially in the Kenyan Jua Kali industry, those teeth are repaired via weld filing and then machined/shaped to the necessary sizes and shapes. In another case, crankshaft bearings tend to wear over time when exposed to excessive heat, especially when the coolant is ineffective [14,15]. Similarly, burner pipes operate at high temperatures, and as such, pipes develop cracks and later fail [16]. In such instances, repair welding is used as a surface engineering technique to rehabilitate the structures.

Research on repair welding as a surface engineering of steel and other engineering components has received little attention. According to [16], the application of welding to repair worn-out steel burner pipe exposed to a temperature of 850°C was investigated. They observed that the burner pipe had cracks on the inner sides after thermal exposure. Similarly, [10] repaired worn-out gear shafts by using welding. Also, a worn-out low carbon steel shaft was repaired using discontinuous arc welding [11]. The welding repair technique has been used widely in the repair of boilers. For instance, a boiler bottom panel damaged due to exposure to low temperature and sulphuric acid [17] was repaired via welding.

Although there are a couple of studies on repair welding as a surface engineering method, there are few reports on the effects of various welding parameters on the coating properties (quality-parameter interactions). This study studied the coating properties as affected by welding parameters. The welding was undertaken at different currents to establish current influence on the welding process. This article reports on the microstructure, mechanical, and corrosion properties as affected by welding parameters. The study provides a scientific resource to justify (and probably make suggestions concerning) the use of repair welding as a surface engineering technology in the Jua Kali (small-scale) industry in Kenya and the rest of the world.

2. EXPERIMENTAL

The test samples were taken from a mild steel plate (substrate material was AISI 1045). Before coating, the samples were ground using silicon carbide papers, then cleaned with acetone and dried. The test samples were then coated using a stainless-steel electrode (Castolin 6825) through TIG welding using a TIG 2200i AC/DC machine. Stainless steel rods were used because they exhibit high hardness, corrosion, and wear resistance properties compared to mild steel. As such, repair welds obtained would have improved mechanical properties. The coating was taken at various AC and DC currents of 40 A, 50 A, 55 A, 60 A, 65 A, and 70 A. Table 1 shows the chemical composition of the substrate and the welding electrode.

Table 1. Chemical composition of Castolin 6825 and AISI 1045 [16].

Element	Chemical composition in Castolin 6825 (%)	Chemical composition in AISI 1045 (%)
Iron (Fe)	1.84	98.35
Titanium (Ti)	-	0.05
Nb+Ta	3.4	-
Copper (Cu)	0.01	0.03
Tungsten (W)	-	0.033
Sulfur (S)	-	0.01
Carbon (C)	0.01	0.312
Nickel	63.52	-
Silicon (Si)	0.2	0.189
Chromium (Cr)	20.95	0.025
Manganese (Mn)	0.69	0.852
Molybdenum (Mo)	-	0.033
Vanadium (V)	-	0.04
Aluminum (Al)	-	0.037
Phosphorus (P)	0.005	0.039

Both AC and DC were chosen based on the capability of the TIG welding equipment; the machine can operate with both DC and AC. Additionally, these two currents are used in repairing steel components (shafts, gears, pipes) in the Kenyan Jua Kali industry. As such, the two currents were considered in this study to imitate the process of repair welding. The welding parameters are shown in Table 2.

Table 2. Welding parameters combination as per $2^1 \times 6^1$ full factorial.

S/NO	Levels	
1	DC	40 A
2	DC	50 A
3	DC	55 A
4	DC	60 A
5	DC	65 A
6	DC	70 A
7	AC	40 A
8	AC	50 A
9	AC	55 A
10	AC	60 A
11	AC	65 A
12	AC	70 A

Using a diamond cutting tool, the coated samples were sectioned from the main substrate and divided into 5 mm by 3 mm cross-sections. The coated sample specimens were hot mounted, after which they were ground and polished using the standard metallographic procedures. The following analyses were done using standard procedures: wear, microhardness, corrosion, and optical microscopy. Samples were etched with Villella's reagent to reveal the microstructures. The depth of penetration and coating thickness were analysed using ImageJ software. Ten different readings were measured for each case, and their average values were determined.

The wear test was carried out using a tribometer. A ball of 6.350 mm diameter made of E5200 alloy steel of grade 25 with hardness ranging between 64-66 RC was used to undertake the dry reciprocating and sliding wear. A normal load of 30 N, a reciprocating time of 30 minutes, a scratch length of 5 mm, and a reciprocating speed of 4 mm/second were used as the wear test parameters.

The coated samples were evaluated for corrosion behaviour using an accelerated environment of 5% wt NaCl. The electrolyte/medium was kept at 80°C in a water bath. The tests were conducted at this temperature because some of the components repaired through welding, such as gears and crankshafts, operate at temperatures between 80°C – 85°C. The samples were initially weighed before the corrosion test and then exposed to the corrosion medium for one hour, after which they were wiped, dried, and weighed. This process was repeated on all samples after 2 hours, 3 hours, 4 hours, and 5 hours. After 5 hours, all samples were removed from the water bath, dried, and examined for corrosion mechanism on a stereomicroscope.

The hardness of the coated samples was measured using a Digital Rockwell Hardness Tester. The hardness values were measured across the samples, starting from the substrate section to the surface of the coating. The hardness values were taken from five different points at 0.5 mm from each other. On each point, five readings were taken and their averages calculated.

3. RESULTS AND DISCUSSION

3.1 Microstructural Analysis

The optical microscopic images of the coated samples taken along the coating-substrate cross-section were analysed. The images showed five distinct regions: coating, fusion, skirt, heat-affected zone (HAZ), and substrate, as shown in Figure 1. The fusion region/interface is where the coating material was fused to the substrate. The region is composed strictly of melted materials. The term skirt was adopted from additive manufacturing, and it is the region that occurred between the coating and the interface. Therefore, in this study, the skirt is the first layer of the coating material deposited on the substrate at the beginning of the welding process. Similarly, the heat-affected zone refers to the non-melted section of the substrate that changed material property due to its exposure to welding temperatures.

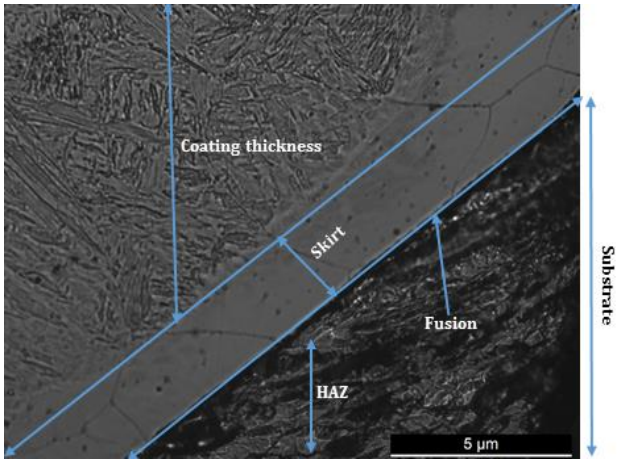

Fig. 1. The microstructure shows various regions of the sample coated at 60 A direct current. The optical microscopic image was taken along the coating-substrate cross-section.

Figures 2 and 3 show the porosity features on the mild steel samples coated using direct currents of 40 A and 50 A, respectively. For 40 A, the porous features were seen in the coating region but not in other weld regions. The reason may be due to different temperature distribution across the weld region of the sample. The temperature at the coating region (weld metal) was higher than in other weld regions. This coating region was more exposed to the atmosphere, where gasses were trapped within the melt pool, causing bubbles that resulted in porosity [18,19]. Generally, the visibility of porosity was clearer at 50 A than at 40 A. An increase in current resulted in increased heat, which caused porosity formation. At 50 A, the porosity distribution was even in the coating region, heat affected zone, fusion region, and skirt region, as shown in Figure 3.

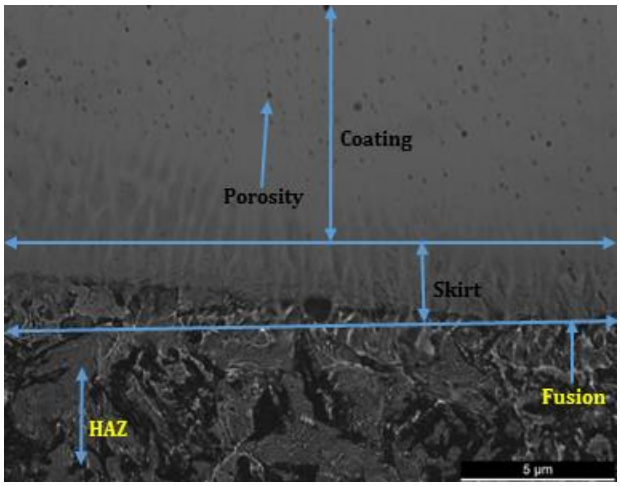

Fig. 2. Illustration of the porosity features on a sample coated at a direct current of 40 A. The optical microscopic image was taken along the coating-substrate cross-section.

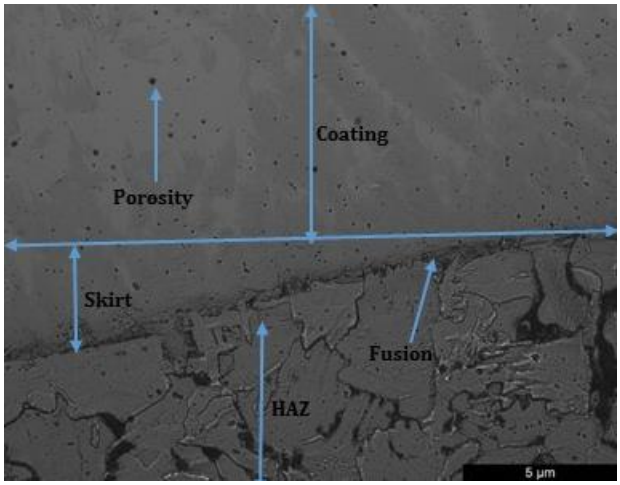

Fig. 3. Illustration of the porosity features on a sample coated at a direct current of 50 A.

Figures 4 and 5 show the samples coated at direct currents of 55 A and 60 A, respectively. The visibility of porosity at 55 A was lesser than that at 50 A. At 55 A. Penetration depth was higher (2.592 mm) than at 50 A (2.328 mm). Hence, causing a lower porosity formation. Therefore, at 55 A, most of the melt pool had penetrated the substrate, and little was left on the surface to trap gases (oxygen) and create porosity. At 60 A, the visibility of pores was observed compared to 55 A. An increase in temperature heated the weld pool, which absorbed gas particles into the molten weld pool. Once the pool solidified, porosity was formed.

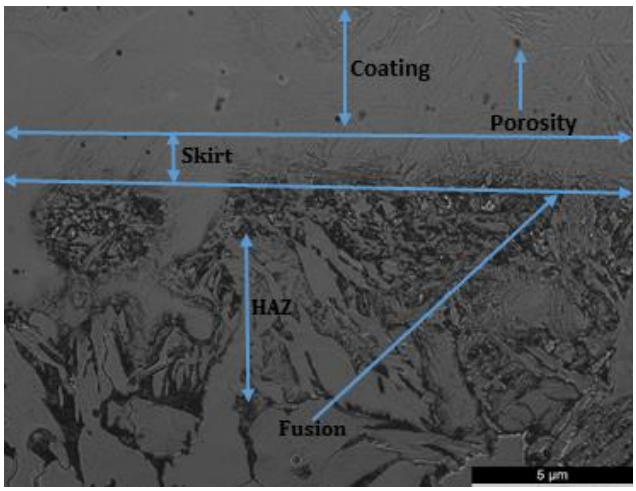

Fig. 4. Porosity in the sample coated at 55 A DC. The optical microscopic image was taken along the coating-substrate cross-section.

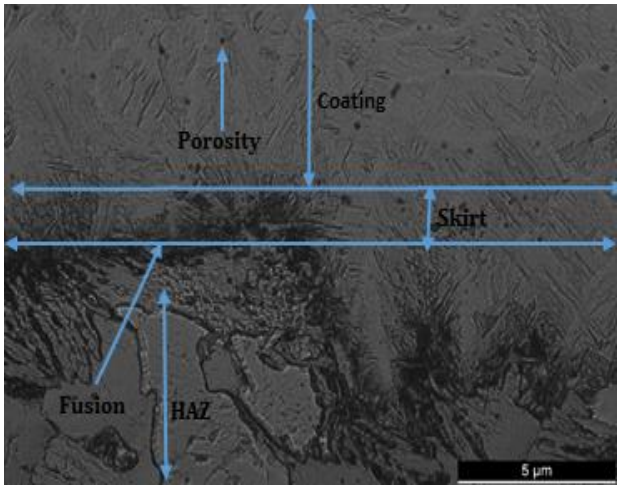

Fig. 5. Porosity in the sample coated at 60 A DC. The optical microscopic image was taken along the coating-substrate cross-section.

Figures 6 and 7 show the samples coated at 65 A and 70 A, respectively. At 65 A, the visibility of porosity was more evident than at 60 A. This

behaviour was observed because as the welding/coating current increased, more heat energy was introduced to the melt pool. As such, massive heat resulted in more gas bubbles trapped within the melt pool, which caused porosity. At 70 A, porosity was less visible than that at 65 A. Welding using DC provided fast and steadier heating than AC. At 70 A, too much heat made the welder move very fast; therefore, less melt pool was formed on the surface to trap bubbles to create porosity. This explains why 70 A had less porosity than 65 A.

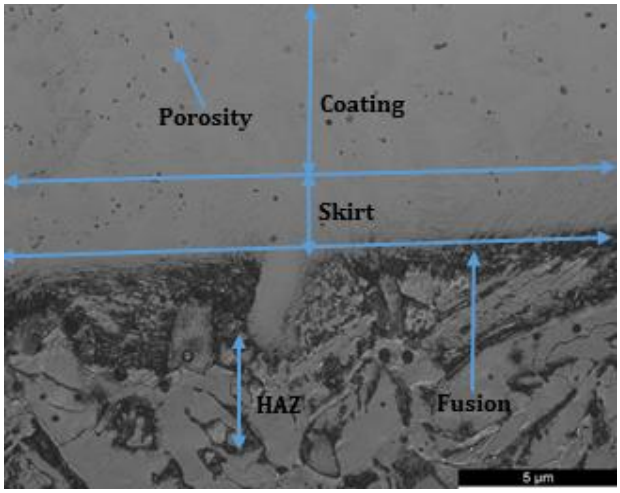

Fig. 6. Porosity in the sample coated at 65 A direct current. The optical microscopic image was taken along the coating-substrate cross-section.

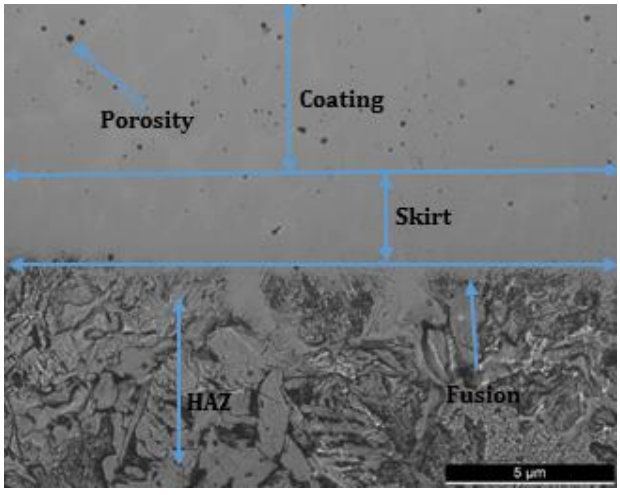

Fig. 7. Porosity in the sample coated at 70 A direct current. The optical microscopic image was taken along the coating-substrate cross-section.

For alternating current, the porosity features were observed in the samples coated using 40 A 50 A, as shown in Figures 8 and 9. At 40 A, the porosity was distributed throughout the coating region. In contrast, the skirt, heat-affected zone, and fusion region had no porosity. At 50 A, the porosity was more visible than at 40 A. Here, the porosity features were evenly distributed at the coating and skirt regions with limited distribution at the fusion and heat-affected zones.

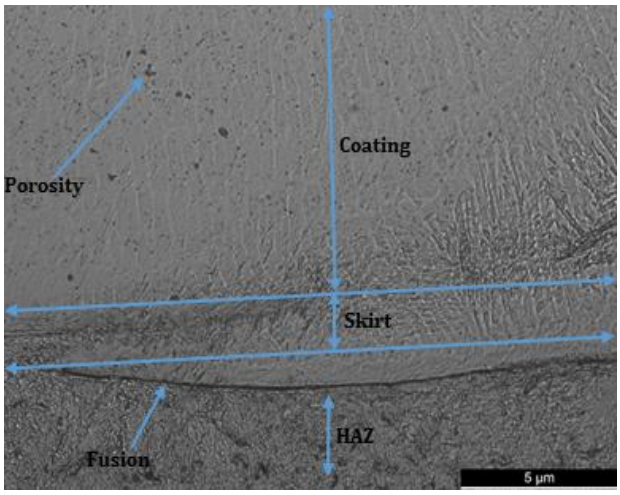

Fig. 8. The mild steel sample coated at 40 A alternating current. The optical microscopic image was taken along the coating-substrate cross-section.

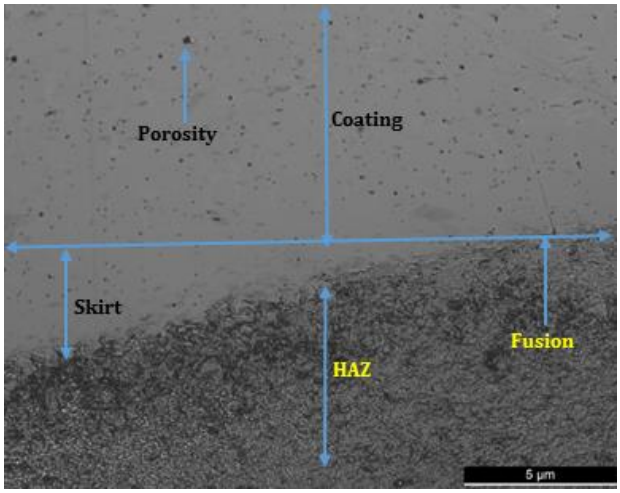

Fig. 9. The sample coated at 50 A alternating current. The optical microscopic image was taken along the coating-substrate cross-section.

Figures 10 and 11 show the samples coated at 55 A and 60 A, respectively. When 55 A was used, the porosity on the coating region was less visible than that at 50 A. Porosity features were also observed in the heat-affected zone, fusion, and skirt region. At 60 A, the porosity was more visible and closely distributed at the coating, skirt, and fusion regions with limited distribution in the heat-affected zone.

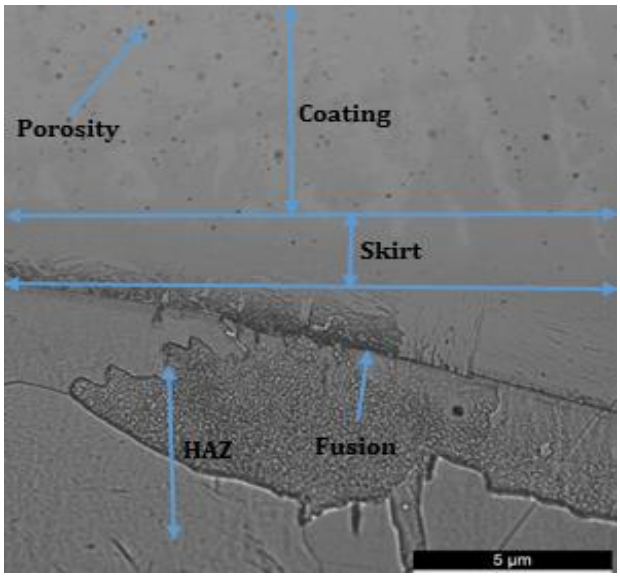

Fig. 10. Mild steel sample coated using 55 A TIG alternating current. The optical microscopic image was taken along the coating-substrate cross-section.

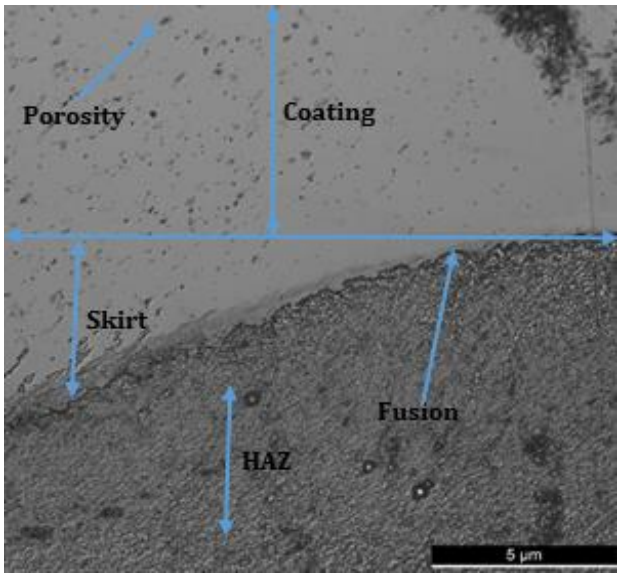

Fig. 11. Illustration of the mild steel sample coated using 60A TIG alternating current. The optical microscopic image was taken along the coating-substrate cross-section.

The samples coated at 65 A and 70 A are shown in Figures 12 and 13, respectively. At 65 A, porosity at the coating region was less visible than at 60 A. The porosity, in this case, was evenly distributed in the coating region, whereas there was a limited distribution in the fusion region and the skirt region. At 70 A, porosity at the coating, skirt, heat-affected zone, and fusion was more visible than at 65 A. The presence of porosity in the heat-affected zone at 60 A, 65 A, and 70 A is attributed to increased welding temperatures, resulting in more heat input.

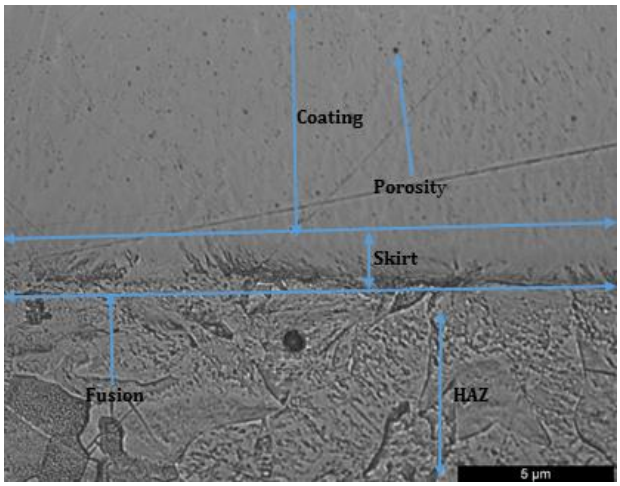

Fig. 12. The mild steel sample coated at 65 A alternating current. The optical microscopic image was taken along the coating-substrate cross-section.

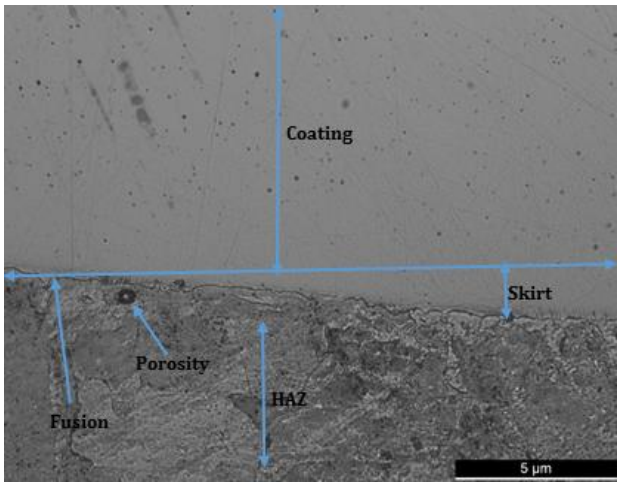

Fig. 13. the mild steel sample coated at 70 A alternating current. The optical microscopic image was taken along the coating-substrate cross-section

3.2 Depth of penetration (DOP)

The results showed that 65 A direct current had the highest penetration depth, as shown in Figure 14. The relationship between DOP and welding current exhibited a hook-like shape. A quadratic polynomial with a regression coefficient of 0.9538 was used to fit this trend. As the current increased from 40 A to 55 A, the depth of penetration increased. The observation is attributed to increased amperage, which increased DOP as more melt pool was heated (more heat melts more melt pool) and penetrated the substrate. However, from 65 A to 70 A, too much current caused the welder to move too quickly. As such, there was lower metal deposition on the surface. At 40 A and 70 A, the DOP values were closer than at 50 A, 55 A, 60 A, and 65 A (as indicated by the

error bars in Figure 14). Closer DOP values indicated an almost uniform penetration of the melt pool into the substrate. Unequal penetration indicated the presence of unequal weld beads/coatings thickness.

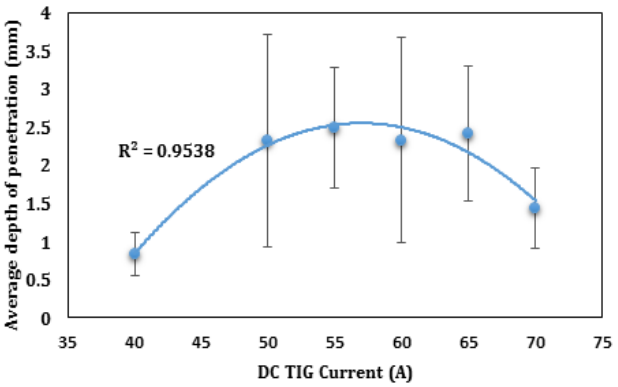

Fig. 14. An illustration of the relationship between the depth of penetration and TIG direct current.

The average depth of penetration when the alternating current was used was observed to be lowest at 55 A and highest at 70 A, as shown in Figure 15. As shown, the depth of penetration generally increased with the increasing current. As the coating current increased, much heat energy was introduced into a coating zone. As such, a lot of melt pool penetrated the substrate, and large depths of penetration were observed. The relationship between DOP and the alternating current was determined using a quadratic polynomial with an accurate closeness of 0.7766. The error bars in Figure 15 indicated that a more significant deviation of DOP occurred at 40 A, 60 A, 65 A, and 70 A. However, at 50 A and 55 A, lesser variations of DOP values were observed. An almost uniform penetration occurred at 50 A and 55 A.

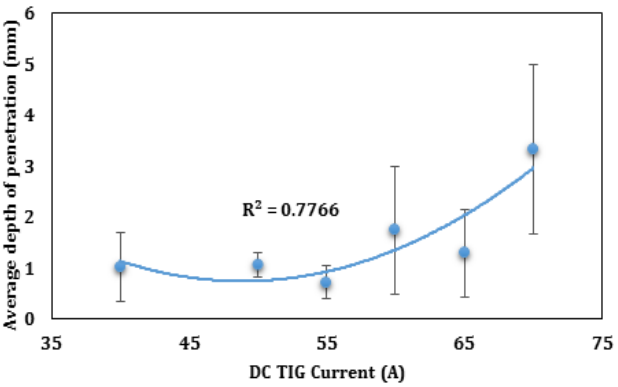

Fig. 15. A graph of the average depth of penetration versus alternating current

The trend in Figure 15 is not uniform (a perfect curve was not formed) as the alternating current kept changing during the coating process. The alternating current rose to a certain voltage, which heated the melt pool and dropped to zero. Therefore, the melt pool cooled a bit more, after which the voltage rose again. This way, the penetration of the melt pool was affected as the temperature kept changing. For direct current, however, the voltage remained at its maximum. Therefore, heating was steadier and faster, leading to continuous heating of the melt pool and, hence, better penetration. As such, coating using direct current had a higher depth of penetration values compared to coating using alternating current

3.3 Coating thickness

Figures 16 and 17 show the coating thickness results for direct and alternating currents, respectively. As shown in Figure 16, the coating thickness generally decreased with increasing current. The highest coating thickness was observed at 40 A. As the coating current increased (heating was fast and steadier), more melt pool penetrated the substrate, leaving less deposited on the surface to form the coating thickness. During welding, an increase in current caused an increase in heat input. The welder moved faster, causing lower metal deposition on the surface. The variations of the coating thickness show that the coating thickness was uninformed.

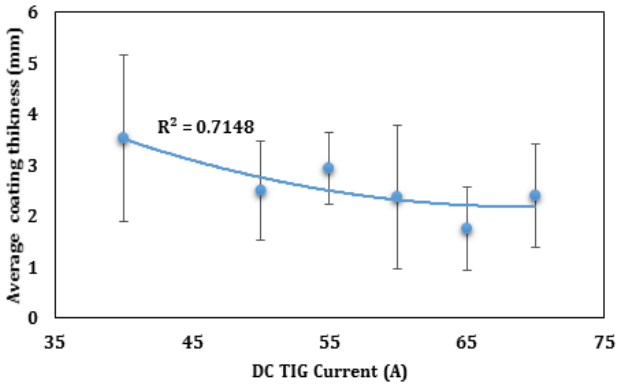

Fig. 16. A plot of the average coating thickness versus direct current.

As shown in Figure 17, 55 A had the highest coating thickness. Generally, the coating thickness decreased with the increasing current (except for 55 A, which did not follow the trend). As the welding current increased, an increase in heat input melted the melt pool, which penetrated the substrate. A little melt pool was left on the surface to form coatings. The error bars in Figure 17 indicate that the deviations of the coating thickness

at each current were massive. The non-uniformity in the trend (the curve shown in Figure 17 is not perfect) was caused by the variation of the alternating current voltage, which resulted in variable heat inputs—the coating thicknesses formed at each current varied from the average thickness. Generally, the samples coated using direct current had higher coating thickness than alternating current coated samples. The observation is attributed to the steady and fast heating effect provided by the direct current, which led to more melt pool deposited on the surface.

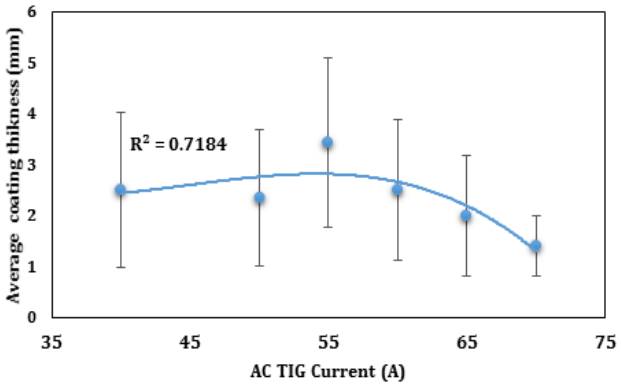

Fig. 17. A graph of average coating thickness versus alternating current.

3.3 Hardness test results

The hardness of the coated samples is shown in Figures 18,19, 20, and 21. Figure 18 shows that 40 A direct current had the highest hardness values. For direct current, the hardness values ranged from 69.08 HRB to 121.92 HRB. Figure 19 shows that the sample coated at 40 A (alternating current) exhibited the highest hardness values. The hardness values for alternating current-coated samples varied from 72.5 HRB to 117.2 HRB.

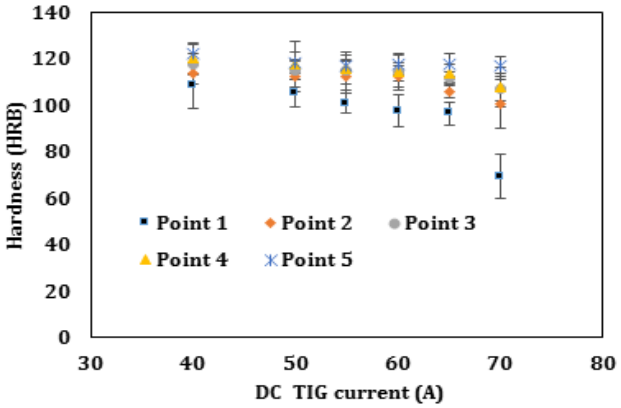

Fig. 18. A graphical representation of the relationship between hardness measured at various points on the coated samples and the coating current (DC).

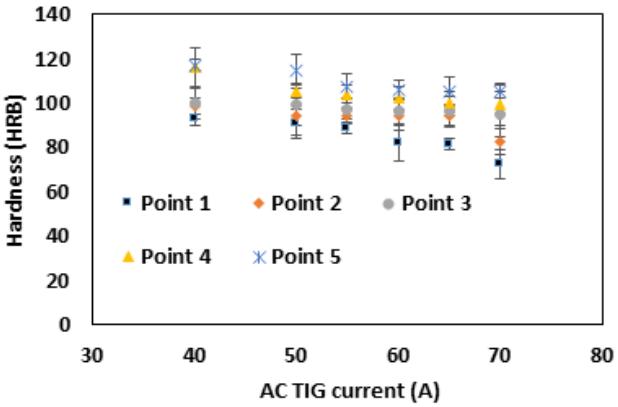

Fig. 19. A graphical representation of the relationship between hardness measured at various points on the samples coated using AC.

The hardness values decreased with increased current (alternating and direct currents). As the welding current increased, the temperature of the coating process increased. High temperature resulted in more melt pool and slow cooling, leading to nucleation and grain growth. Large grains are associated with lower mechanical strength following Hall the Petch's law. As reported by [20], the hardness values of welded low–carbon steel decreased with increased welding current.

The hardness increased from the substrate to the coating's surface for alternating and direct currents, as shown in Figures 20 and 21. The coating surface showed higher hardness than at the interface (point 3) and the centre of coated samples (point 4). The behaviour may be due to the rapid solidification of the surface caused by exposure to the atmosphere. As such, there was the formation of fine-grained structures and chemical homogeneity, and according to existing literature, fine-grained structures are known to exhibit improved hardness [21].

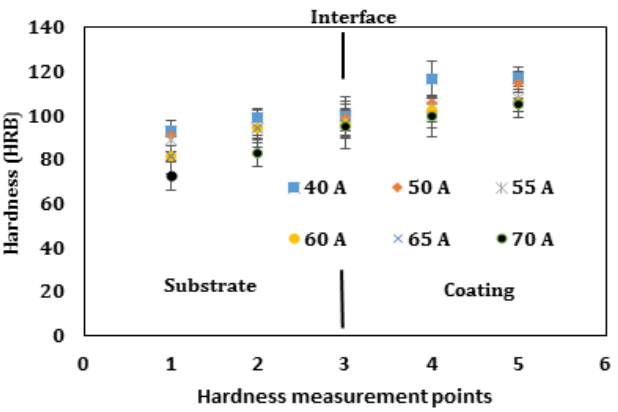

Fig. 20. A graphical representation of the relationship between hardness measured at each welding current at various points on the coated samples for AC.

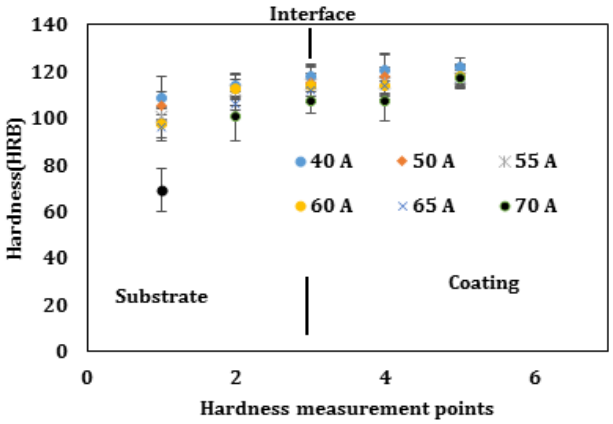

Fig. 21. A graphical representation of the relationship between hardness measured at each welding current at various points on the coated samples for DC.

3.4 Corrosion test results

During the corrosion test, an accelerated environment of 5% wt NaCl and a temperature of 80 °C was simulated. The test environment was a simulation of the actual conditions, which reflects the working conditions under which some components such as gears and crankshafts operate (the maximum temperature allowable for conventional automatic transmission systems is between (80-100 °C) [22] When the temperature increases, the rate of corrosion tends to increase. The corrosion process is an electrochemical process. A temperature increase causes electrons to move faster, making their collision quick and frequent [23]. The electrolyte (in this case, NaCl) provided the chloride ions that accelerated the corrosion rate.

The weight of the samples subjected to corrosion was measured using a weighing balance before the experiment and after every 1 hour for five hours. For each current, the calculated accumulative weight change after 5 hours results obtained was presented graphically in Figure 22. The relationships between the weight loss for samples and current (both alternating and direct) had almost similar trends. The samples coated at 60 A (direct current) and 40 A (alternating current) exhibited the highest weight loss, meaning they corroded the most. This observation is related to porosity and coating thickness results. The sample welded at 60 A DC showed a rapid weight loss compared to samples coated at 50 A and 65 A direct currents. The observation occurred because the 50 A sample had a higher coating thickness than the 60 A sample. Similarly, the presence of porosity in the 60 A sample was higher than in the 65 A sample.

During welding, porosity occurs due to unwanted or un-melted particles in the molten metal. Hence, porosity causes poor coating cohesion, resulting in a higher corrosion rate. Lower coating thickness values enhance higher corrosion rates as thin coatings are prone to corrosion attacks.

The samples coated at 65 A (alternating current) and 55 A (direct current) had better corrosion resistance than the other test samples. The microstructure revealed a low porosity at 55 A and 65 A welding currents. The coating thickness and DOP values were slightly higher at 55 A and 65 A test currents. Hence, the coatings showed better corrosion resistance properties. The direct current-coated samples had better corrosion resistance properties. The higher corrosion resistance behaviour was due to a higher coating thickness. Thicker coatings reduce the rate of corrosion of the substrate (mild steel) [24]. The better corrosion resistance for direct current can result from high DOP values.

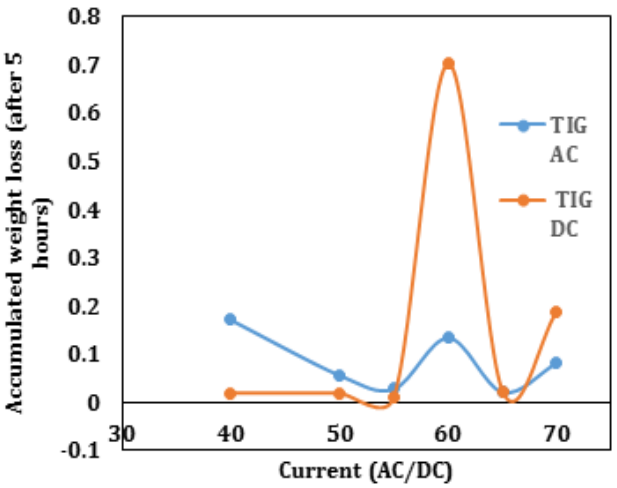

Fig. 22. A graphical representation of the weight loss (after 5 hours) for coated samples against the welding current used.

The results for weight loss after each hour for the test currents are shown in Figures 23 and 24. An increase in time caused a slight weight loss for all the test currents except 40 A for the alternating current (Figure 23). In this case, the weight loss increased significantly after two hours and became almost constant after three hours. For the direct current, at 60 A, the weight loss after every hour increased with increasing time for the first two hours, after which it assumed a constant trend. The trends observed in Figures 23 and 24 are related to lower values of DOP, coating thickness, and the presence of porosity features.

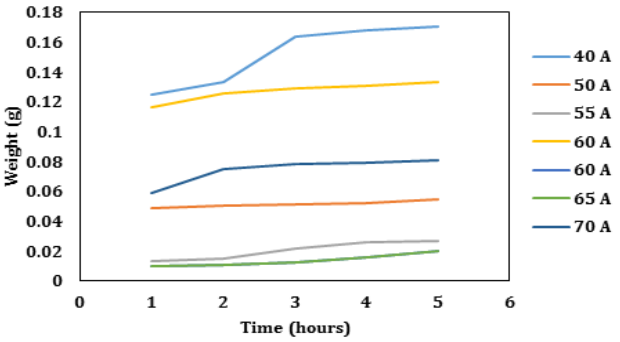

Fig. 23. An illustration of the variation of weight loss after every hour for AC.

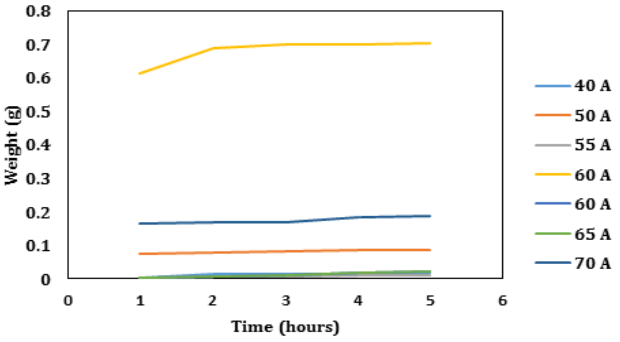

Fig. 24. An illustration of the variation of weight loss after every hour for DC.

After 2 hours, the substrate region of the samples exhibited black and grey patches on their surfaces. The sample surfaces had a rough brownish product between the third and the fourth hour. Towards the end of the experiment, the brown product was deposited at the bottom of the beaker. This observation indicated that corrosion was due to erosion that resulted in water turning brownish. After cleaning, the corroded samples had pits, suggesting that pitting corrosion was dominant in this study. The pitting/cavities were due to the reaction of NaCl solution. The aggressive chloride ions in the solution reacted with the coating surface, causing a localised breakdown of the coating protective passive layer. This chemical reaction caused the formation of tiny holes (pits). As the rate of corrosion increased, the pits grew into cavities.

3.5 Wear test results

Figures 25 and 26 show the typical coefficient of friction curves (CoF) of coatings (coated at 40 A, both AC and DC, respectively) generated at the same sliding speed and load). All other coated samples were observed to assume similar trends. The wear process underwent three stages as the sliding proceeded: stages 1, 2, and 3. Stage 1 is the run-in stage, and stage 2 is the transition region between the run-in and steady-state stages (stage 3). The wear started with the run-in stage (rapid initial wear), during which the steady-state conditions were building up. The mating surfaces (the coating and the sliding ball) conformed during the run-in stage. The load became more favourably distributed over the surfaces resulting in rapid wear and increased CoF. Wear and CoF increased slowly. Generally, the CoF's running in periods increased initially, then decreased to reach nearly a steady-state region. The initial contact between the coating and the abrasive ball occurred at a few asperities, which resulted in high contact stress. When the wear proceeded (increased time), the contact area increased, causing a reduction in contact stress and CoF. An increase in sliding caused the wear debris generated due to plastic deformation to cover the surface, causing an increase in adhesion, increasing CoF. CoF variations resulted in the formation and delamination of the tribolayer and abrasive particles from the sliding ball. A higher coefficient of friction values occurred when the AC was used compared to DC. The observation can be attributed to the higher hardness values determined for direct current test samples. According to existing literature, wear resistance increases with increasing hardness [25].

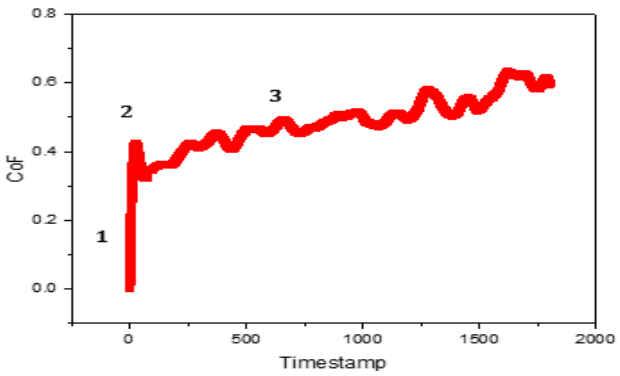

Fig. 25. A graphical representation of CoF against the timestamp for the wear measured on the sample welded using 40 A AC.

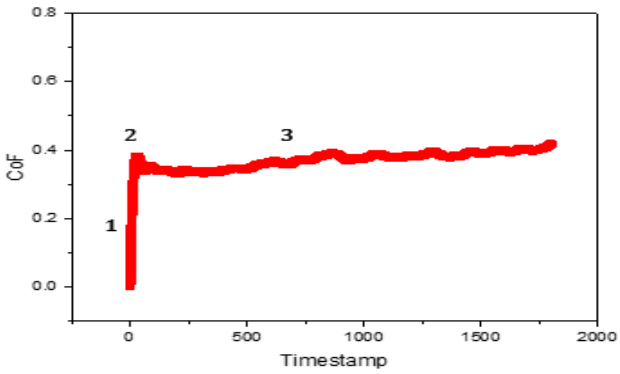

Fig. 26. A graphical representation of CoF against the timestamp for the wear measured on the sample welded using 40 A DC.

The wear depth was plotted against the welding current, as shown in Figures 27 and 28. As shown, there was no linear relationship between the wear depth and the welding current used. The highest wear depth was observed at 55 A AC and 65 DC. These samples had lower coating thicknesses. As such, they experienced the most wear as the coating thickness was not thick enough to protect them from wearing out. The sample coated at 55 A alternating current experienced a greater wear (with a depth of wear above 48 microns) than at 65 A direct current (depth of wear is below 46.5 microns). The difference can be due to 55 A (alternating current) having a coating thickness of 0.719 mm, whereas, at 65 A (direct current), the coating thickness was 1.755 mm. The larger coating thickness resulted in better wear resistance properties. Also, hardness values were slightly higher at 65 A (direct current) than at 55 A (alternating current). Therefore, the higher hardness increased the wear resistance of the sample.

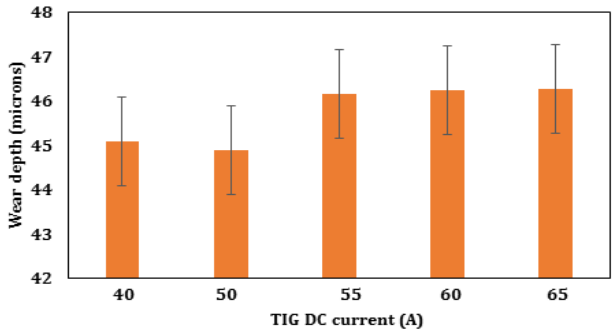

Fig. 27. Illustration of the variation of the depth of wear and welding current for DC.

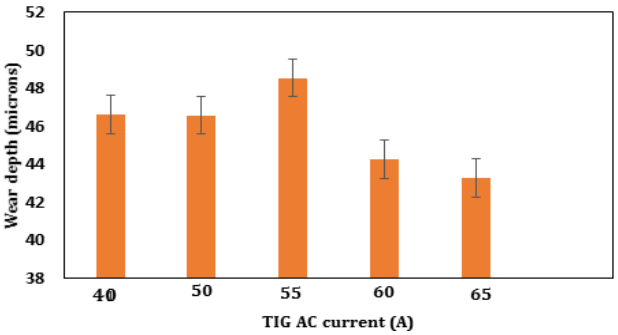

Fig. 28. Illustration of the variation of the depth of wear and welding current for AC.

Optical micrographs of the wear tracks were analysed to identify the mechanism of wear. Figure 29 shows the wear track of a sample coated at 40 A alternating current. As shown in Figure 29, the wear mechanisms were: abrasive (grooving), adhesion, and fatigue wear/delamination.

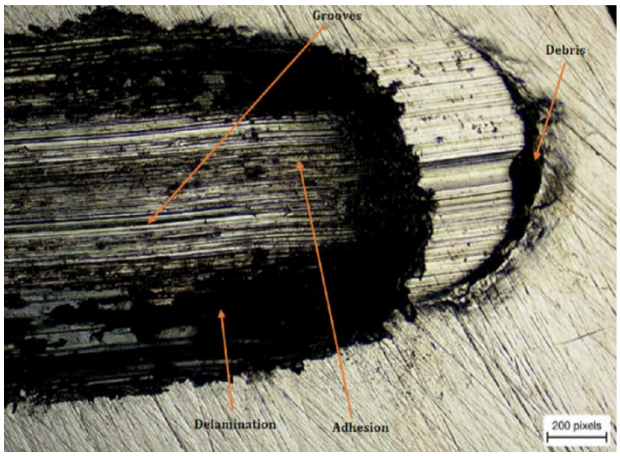

Fig. 29. The micrograph of the wear track for the sample welded using 40 A AC.

The white patches represent grooves, which there were deeper cuts of the coating. The black sections at the sides of the sample show the delamination and wear debris. In this case, the micrograph showed more grooves than delamination spots. There was also adhesion transfer which led to debris at the side of the coating. These results indicated that the sample experienced more abrasion and adhesive wear and lesser delamination wear. The 50 A coated sample (shown in Figure 30) experienced more abrasion and adhesion than delamination. The sample would be suitable for applications that require protection against delamination wear.

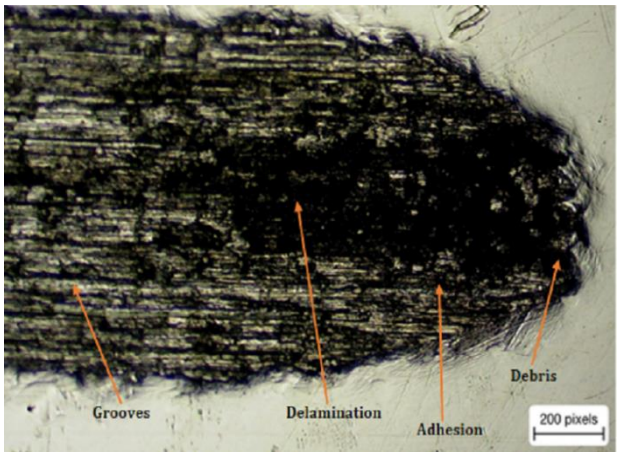

Fig. 30. The micrograph of the wear track for the sample coated using 50 A AC**.**

Figures 31, 32, and 33 showed that delamination occurred at 55 A, 60 A, and 65 A distributed throughout the samples with minor grooves and adhesion transfer. These results implied that at alternating currents of 55 A, 60 A, and 65 A, the coated samples were more vulnerable to delamination than abrasion and adhesion wear.

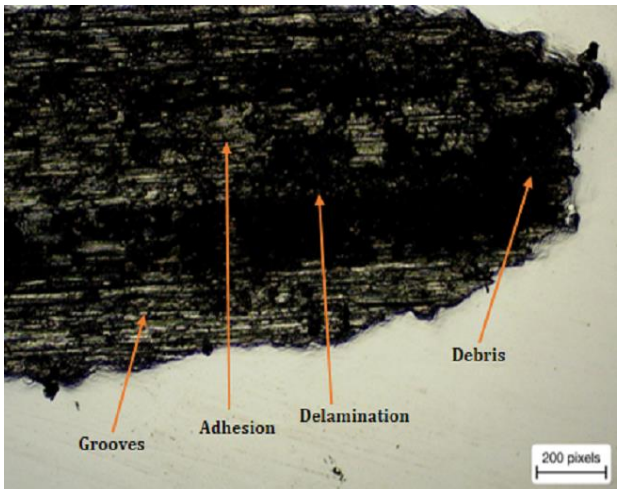

Fig. 31. The micrograph of the wear track for the sample coated using 55 A alternating current.

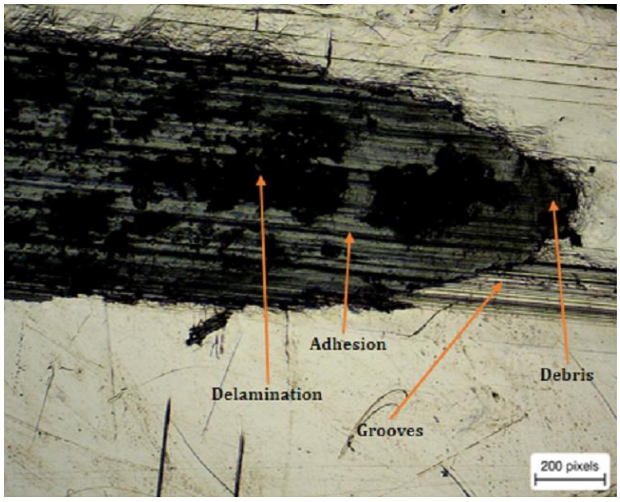

Fig. 32. A micrograph of the wear track for the sample welded at 60 A alternating current.

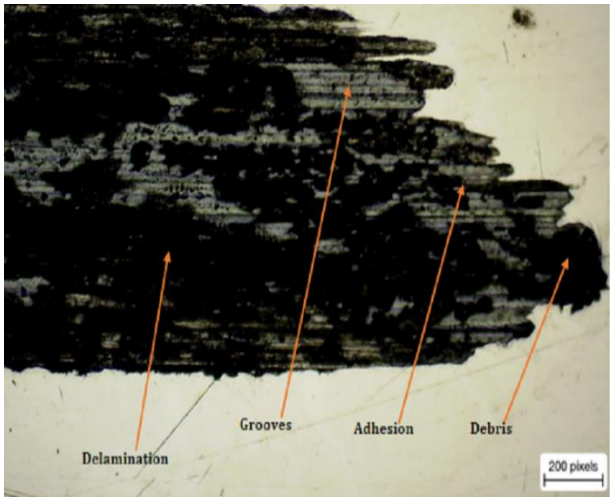

Fig. 33. A micrograph for wear track of a sample coated using 65 A AC.

Figure 34 shows the micrograph of the wear track for a sample coated at 40 A direct current.

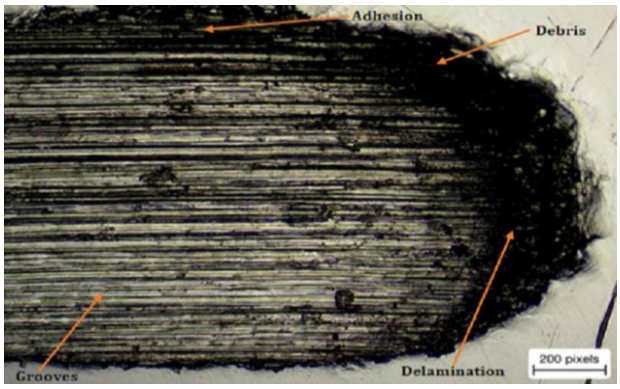

Fig. 34. The micrograph of the wear track for the sample coated using 40 A DC.

The sample coated at 40 A direct current displayed many grooves and adhesion wear with minor delamination. Also, at 50 A (Figure 35), 55 A (Figure 36), 60 A (Figure 37), and 65 A (Figure 38), large grooves, adhesion transfer, and delamination patches were observed. These wear features indicate that the samples were vulnerable to the three wear mechanisms (adhesion, abrasion, and delamination).

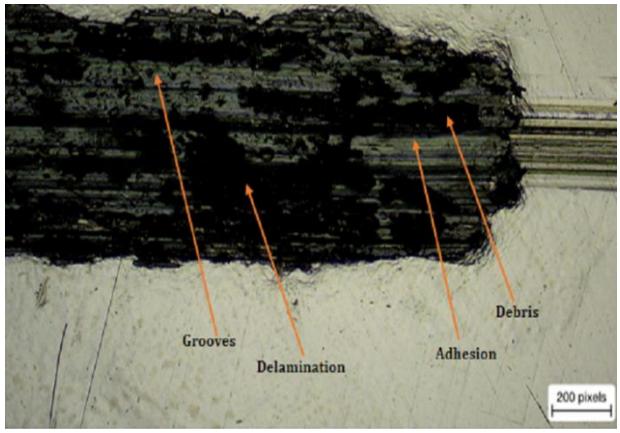

Fig. 35. A micrograph showing the wear track of a sampled welded using 50 A DC.

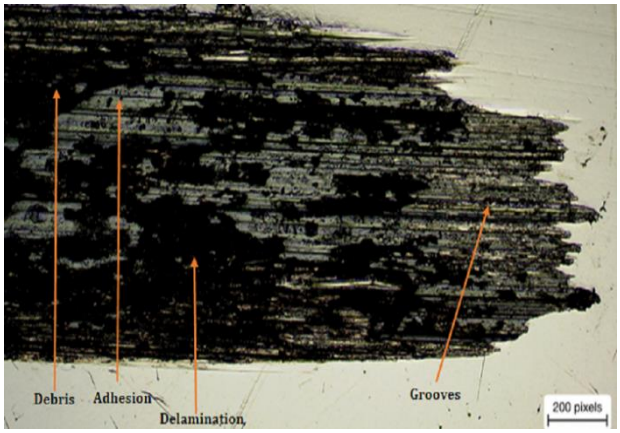

Fig. 36. A micrograph for the wear track of the sample coated at 55 A direct current.

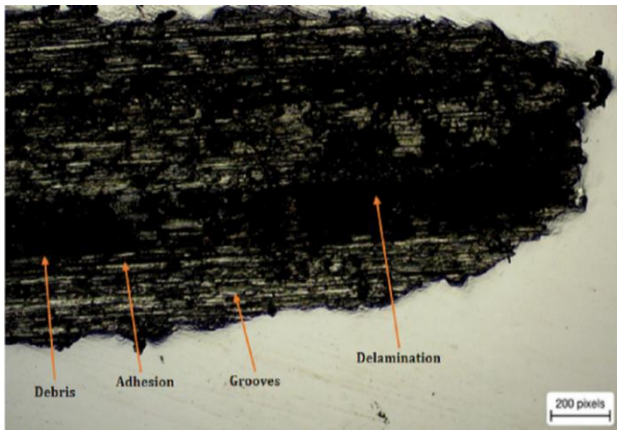

Fig. 37. A micrograph showing the wear track of sample welded using 60 A direct current.

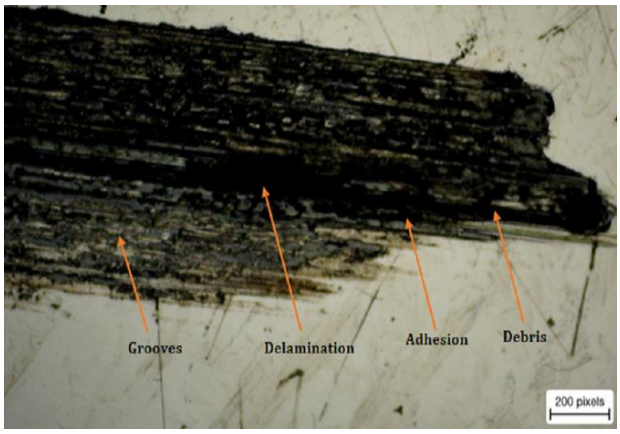

Fig. 38. A micrograph for the wear track for the sample coated at 65 A DC**.**

At 70 A, a combination of grooves and adhesion wear was observed with minor delamination (as shown in Figure 39). Therefore, the sample was vulnerable to adhesion and abrasion wear, making it suitable in applications where protection against delamination attacks is required.

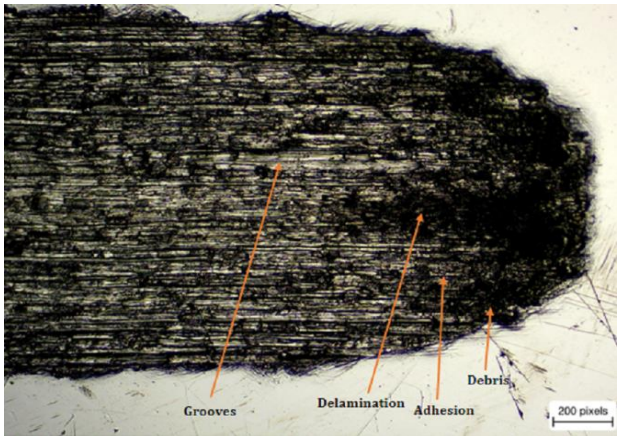

Fig. 39. A micrograph of the wear track for the sample welded using 70 A DC.

During the wear test, the grooves (abrasion) occur when particles of the sliding ball penetrate the coating surface during contact. Hence, surface damage/cutting occurs by the grooving of contact surfaces. The adhesion wear observed occurs when the material removed (through abrasive wear) was pressed against the coatings and created wear debris. Delamination occurs due to surface fatigue due to a continuous sliding action. Therefore, the subsurface cracks develop and propagate to connect. Later, the developed cracks reach the surface and generate wear particles. The particles at the sliding surface were delaminated, then pressed against the back of the coatings to create grooves. The substrate surface was not visible in the micrographs of the wear tracks. This observation was because the results of the average depths of wear encountered in this study were less than the coating thickness of the samples. Therefore, the wear experienced by the coated samples studied was not severe enough to expose the surface of the substrate. The study revealed that the coated test samples would suit wear resistance applications.

4. CONCLUSION

TIG welding method of repairing steel components with stainless steel was studied. Thick coatings were deposited on substrates using TIG welding at selected operational process variables. The coated samples were characterised for microstructure, hardness, wear, and corrosion properties. The following observations and conclusions were drawn:

1. The porosity in the coated samples increased with increasing currents for both AC and DC. Therefore, lower currents should be used to minimize porosity.
2. At currents below 40 A, the welding rod stuck onto the substrate. Above 70 A, there was sputtering and overheating, leading to local substrate melting; therefore, repair welding should be conducted at currents between 40 A-70 A.
3. In applications where the largest coating thickness is desired, the welders should use 65 A (DC) or 70 A (AC) as they display the largest values of coating thickness.

4. Repair welding should be carried out using welding currents of 40 A (DC) and 55 (AC) if large DOP values are needed.
5. The corrosion mechanism encountered was pitting; therefore, the steel structures repaired in the Jua Kali sector are likely to experience the exact corrosion mechanisms.
6. The coated samples experienced adhesion, delamination, and abrasion wear. These are the wear mechanisms likely to occur to the components repaired through welding.
7. To achieve the most excellent wear resistance properties in repair welding, welders should use 50 A (DC) or 65 (AC).
8. The hardness of the coated samples decreased with increasing current (both alternating and direct currents). The hardness increased from the substrate towards the coating. As such, welding is a viable method of repairing steel components as the hardness of the repaired parts is increased.
9. Wear resistance results indicated that the substrate surfaces were not exposed after wear, meaning severe wear did not occur. As such, repairing steel components with stainless-steel welding rod material is sufficient to protect the substrate from extreme surface wear conditions during applications.

Acknowledgment

The authors acknowledge the Dedan Kimathi University of Technology, Kenya, and the University of Johannesburg, South Africa.

REFERENCES

[1] M.N. Muigai, E.T. Akinlabi, F.M. Mwema, *Influence of direct current (DC) on hardness of weld stainless steel coating - A model for mild steel repair,* Materials Today: Proceedings, vol. 44, pp. 1133–1135, 2021, doi: 10.1016/j.matpr.2020.11.230

[2] R.W. Messler, *Overview of Welding Processes*, in T. Lienert, T. Siewert, S. Babu, V. Acoff (Ed.): Welding Fundamentals and Processes, vol. 6a, 2011, doi: 10.31399/asm.hb.v06a.a0005552

[3] P. Kah, R. Suoranta, J. Martikainen, C. Magnus, *Techniques for Joining Dissimilar Materials, Metals and Polymers,* Reviews on Advanced Materials Science, vol. 36, iss. 2, pp. 152–164, 2014.

[4] Z. Pan, D. Ding, B. Wu, D. Cuiuri, H. Li, J. Norrish, *Arc Welding Processes for Additive Manufacturing: A Review,* Transactions on Intelligent Welding Manufacturing, vol. 2, pp. 3–24, 2018, doi: 10.1007/978-981-10-5355-9_1

[5] M.N. Muigai, F.M. Mwema, E.T. Akinlabi, J.O. Obiko, *Surface Engineering of Materials Through Weld-Based Technologies: An Overview,* in S. Roy, G.K. Bose (Ed.): Advanced Surface Coating Techniques for Modern Industrial Applications, pp. 247–260, 2020, doi: 10.4018/978-1-7998-4870-7.ch011

[6] M.N. Muigai, F.M. Mwema, E.T. Akinlabi, J.O. Obiko, *Influence of direct current (DC) on mild steel coating stainless steel rods via TIG welding: A model for the rehabilitation of steel components*, IOP Conference Series on Materials Science and Engineering, vol. 1107, pp. 1–11, 2021, doi: 10.1088/1757-899x/1107/1/012039

[7] K. Kumar, S.C. Deheri, M. Masanta, *Effect of activated flux on TIG welding of 304 austenitic stainless steel*, Materials Today: Proceedings, vol. 18, pp. 4792–4798, 2019, doi: 10.1016/j.matpr.2019.07.467

[8] J.H. Park, Y.H. Kim, H.J. Baek, S.M. Cho, *A Study on Process Development of Super-TIG Welding for 9% Nickel Steel with Alloy 625,* Journal of Manufacturing Processes, vol. 40, pp. 140–148, 2019, doi: 10.1016/j.jmapro.2019.03.017

[9] D. Tanasković, B. Đorđević, S. Sedmak, A. Mihajlo, *The Effect of Exploitation Conditions on the Damage of a Roller Reducer Toothed Shaft and its Repair,* Machine Design, vol. 10, no. 4, pp. 157-162, 2018, doi: 10.24867/MD.10.2018.4.157-162

[10] D. Tanasković, B. Đorđević, U. Tatić, A. Sedmak, M. Opačić, *Repair welding of gear shafts of service rollers at the Železara Smederevo*, in 8th International Scientific Conference IRMES 2017, 7-9 September, 2017, Trebinje, Bosnia and Herzegovina, pp. 365–370.

[11] B.R. Sadeq, B.S. Sahib, M. Alher, *Study of the Effects of welding process on the microstructure of worn carbon steel shaft*, IOP Conference Series on Materials Science and Engineering, vol. 671, pp. 1–10, 2019, doi: 10.1088/1757-899X/671/1/012161

[12] M.S. Tunalioglu, B. Tuc, E*ffect of tooth profile modification on wear in internal gears,* IOP Conference Series on Material Science and Engineering, vol. 351, pp. 1–6, 2018, doi: 10.1088/1757-899X/351/1/012003

[13] M. Amarnath, S. Chandramohan, S. Seetharaman, *Experimental Investigations of Surface Wear Assessment of Spur Gear Teeth,* Journal of Vibrations and Control, vol. 18, iss. 7, pp. 1009-1024, 2012, doi: 10.1177/1077546311399947

[14] L. Witek, F. Stachowicz, A. Załęski, *Failure Investigation of the Crankshaft of Diesel Engine,* Procedia Structural Integrity, vol. 5, pp. 369–376, 2017, doi: 10.1016/j.prostr.2017.07.184

[15] G.H. Farrahi, S.M.H. Gangaraj, S. Abolhassani, F. Hemmati, M. Sakhaei, F*ailure Analysis of a Four Cylinder Diesel Engine Crankshaft Made from Nodular Cast Iron,* The Journal of Engine Research, vol. 22, pp. 21–28, 2011.

[16] D. Tanasković, B. Dordevic, M. Gajin, M. Arandelović, N. Gostović, *Damages of Burner Pipes due to the Working Conditions and its Repair Welding*, Procedia Structural Integrity, vol. 13, pp. 404–409, 2018, doi: 10.1016/j.prostr.2018.12.067

[17] N. Milovanović, B. Dordević, U. Tatić, S. Sedmak, S. Štrbački, *Low-temperature Corrosion Damage and Repair of Boiler Bottom Panel Tubes,* Structural Integrity and Life, vol. 17, no. 2, pp. 125–131, 2017.

[18] J. Huang, R. Turner, J. Gebelin, N. Warnken, M. Strangwood, R. C. Reed, *The effect of hydrogen on porosity formation during electron beam welding of titanium alloys,* in 9th International Conference on Trends in Welding Research, 4-8 June, 2012, Chicago, Illinois, USA, pp. 1–8.

[19] J.E. Blackburn, *Understanding Porosity Formation and Prevention When Welding Titanium Alloys with 1 μm Wavelength Laser Beams*, PhD thesis, University of Manchester, Manchester, UK, 2011.

[20] M.A. Bodude, I. Momohjimoh, *Studies on Effects of Welding Parameters on the Mechanical Properties of Welded Low-Carbon Steel,* Journal of Minerals Materials Charaeterization an Engineering, vol. 03, no. 3, pp. 142–153, 2015, doi: 10.4236/jmmce.2015.33017

[21] F. Alshmri, H. Atkinson, *Hardness of Rapidly Solidified Al-High Si Alloys,* Advanced Materials Research, vol. 476–478, pp. 2476–2480, 2012, doi: 10.4028/www.scientific.net/AMR.476-478.2476

[22] E. Efficiency, *Energy Efficiency and Reliability in Automatic Transmission Systems (High-Temperature Digital Temp Sensor),* available at: https://www.ti.com/litv/pdf/snia017

[23] M. Cao, L. Liu, L. Fan, Z. Yu, Y. Li, E.E. Oguzie, F. Wang, *Influence of temperature on Corrosion Behavior of 2A02 Al Alloy in Marine Atmospheric Environments,* Materials, vol. 11, iss. 2, pp. 1–22, 2018, doi: 10.3390/ma11020235

[24] M.S.N. Idora, M.M. Rahman, M. Ismail, W.B.W. Nik, *Effect of Zinc Coating Thickness on Corrosion Performance of Mild Steel in Atmospheric and Seawater Environment,* Applied Mechanics and Materials, vol. 554, 2015, pp. 213–217, 2014, doi: 10.4028/www.scientific.net/AMM.554.213

[25] D.H. Jeong, U. Erb, K.T. Aust, G. Palumbo, T*he Relationship between Hardness and Abrasive Wear Resistance of Electrodeposited Nanocrystalline Ni–P Coatings,* Scripta Materialia, vol. 48, iss. 8, pp. 1067–1072, 2003, doi: 10.1016/S1359-6462(02)00633-4